AGU PUBLICATIONS

JGR

Journal of Geophysical Research: Earth Surface

RESEARCH ARTICLE
10.1002/2013JF003069

Key Points:
- Water-level measurements recorded across Chandeleur Islands during Isaac
- Higher water levels on bay side caused seaward cross-barrier sand transport
- Hard-to-observe seaward transport deposits are absent in overwash records

Correspondence to:
C. R. Sherwood,
csherwood@usgs.gov

Citation:
Sherwood, C. R., J. W. Long, P. J. Dickhudt, P. S. Dalyander, D. M. Thompson, and N. G. Plant (2014), Inundation of a barrier island (Chandeleur Islands, Louisiana, USA) during a hurricane: Observed water-level gradients and modeled seaward sand transport, *J. Geophys. Res. Earth Surf.*, *119*, 1498–1515, doi:10.1002/2013JF003069.

Received 20 DEC 2013
Accepted 23 JUN 2014
Accepted article online 26 JUN 2014
Published online 15 JUL 2014

Inundation of a barrier island (Chandeleur Islands, Louisiana, USA) during a hurricane: Observed water-level gradients and modeled seaward sand transport

Christopher R. Sherwood[1], Joseph W. Long[2], Patrick J. Dickhudt[1], P. Soupy Dalyander[2], David M. Thompson[2], and Nathaniel G. Plant[2]

[1]U.S. Geological Survey Woods Hole Coastal and Marine Science Center, Woods Hole, Massachusetts, USA, [2]U.S. Geological Survey St. Petersburg Coastal and Marine Science Center, St. Petersburg, Florida, USA

Abstract Large geomorphic changes to barrier islands may occur during inundation, when storm surge exceeds island elevation. Inundation occurs episodically and under energetic conditions that make quantitative observations difficult. We measured water levels on both sides of a barrier island in the northern Chandeleur Islands during inundation by Hurricane Isaac. Wind patterns caused the water levels to slope from the bay side to the ocean side for much of the storm. Modeled geomorphic changes during the storm were very sensitive to the cross-island slopes imposed by water-level boundary conditions. Simulations with equal or landward sloping water levels produced the characteristic barrier island storm response of overwash deposits or displaced berms with smoother final topography. Simulations using the observed seaward sloping water levels produced cross-barrier channels and deposits of sand on the ocean side, consistent with poststorm observations. This sensitivity indicates that accurate water-level boundary conditions must be applied on both sides of a barrier to correctly represent the geomorphic response to inundation events. More broadly, the consequence of seaward transport is that it alters the relationship between storm intensity and volume of landward transport. Sand transported to the ocean side may move downdrift, or aid poststorm recovery by moving onto the beach face or closing recent breaches, but it does not contribute to island transgression or appear as an overwash deposit in the back-barrier stratigraphic record. The high vulnerability of the Chandeleur Islands allowed us to observe processes that are infrequent but may be important at other barrier islands.

1. Introduction

Transport of sand to the back (bay) side of barrier islands by overwash or through storm-induced breaches allows islands to migrate landward (or roll over) as sea level rises [*Leatherman*, 1979, 1981, 1983; *Donnelly et al*., 2006a]. Landward overwash flux (defined to include both of these processes) is a main component of long-term coastal evolution models [e.g., *Cowell et al*., 1995; *Jiménez and Sánchez-Arcilla*, 2004; *Stolper et al*., 2005; *Ashton and Ortiz*, 2011; *Lorenzo-Trueba and Ashton*, 2014]. Other mechanisms of migration and maintenance of barriers include alongshore transport and spit formation, aeolian transport, transport through tidal inlets, biogenic sediment formation in marshes, and fluvial sediment delivery, but these processes are not as tightly associated with rapid changes by storms. Conceptual understanding of the behavior and evolution of barrier islands is closely linked to their origins and their geological and oceanographic settings [*McBride et al*., 2013]. Barrier systems have been classified on the basis of tidal range and wave height [*Hayes*, 1979], morphological response characteristics [*McBride et al*., 1995], and coastal setting [*Inman and Nordstrom*, 1971; *Pilkey*, 2003]. The relative importance attributed to different morphodynamic processes varies among classifications. Sufficient rates of overwash and cross-barrier transport in temporary breaches are especially important to allow narrow barriers to keep pace with sea-level rise [*Leatherman*, 1979]. In addition, an ample supply of sediment from the shoreface is required [*Lorenzo-Trueba and Ashton*, 2014]. The morphologic response to storms, including overwash processes, is increasingly critical to coastal communities as sea levels rise. Initiatives to make coastlines more resilient range from traditional beach nourishment and dune restoration projects, to construction of artificial berms along the Louisiana coast, to much more ambitious proposals to build an entirely new, artificial barrier system along the East Coast of the U.S. (http://www.rebuildbydesign.org/project/wxywest-8-final-proposal/). Successful design and a full understanding

of the implications of these projects require a quantitative understanding of the processes that control the evolution of barrier island systems.

1.1. Swash, Collision, Overwash, and Inundation

The geomorphic impact of storms on barrier island evolution is expected to increase as the elevation of water levels compared to dune heights increases, according to *Sallenger* [2000] and *Stockdon et al*. [2007, 2012]. Four impact regimes are classified as follows: swash, collision, overwash, and inundation. Relatively minor geomorphic changes and rapid recovery times are associated with the swash regime, where sand may be eroded or even deposited on the beach. During the collision regime, dunes may be eroded, and sand may be moved seaward. Greater magnitudes of beach erosion, shoreline retreat, and geomorphic change occur during overwash and inundation regimes. *Sallenger* [2000, p. 894] stated "limited observations suggest that massive net onshore transport occurs with landward migration of sand bodies on the order of 1 km" during inundation. The implication is that the highest water levels are inextricably linked with maximum geomorphic change and shoreward transport of sand.

However, there is evidence that morphologic response does not always increase monotonically with impact regime. *Long et al*. [2014] studied the relationship between storm regime and change in prestorm dune crest elevations. *Long et al*. [2014] reported that dune height changes during the collision regime were constrained to about 10% of the initial dune height and that changes during the overwash regime were much more variable, ranging from 0 to 100%. Interestingly, they noted that although the inundation regime produced the only cases with breaches, the morphologic response to inundation did not always increase with higher levels of inundation. Thus, it is also possible that landward transport does not increase monotonically with the level of inundation, and there is some reason to think that the rate of net landward transport might be highest at some intermediate level when waves can move sediment across the island crest without any seaward return flow over the dune. Once water levels on both sides of the barrier exceed the crest elevations, gradients may exist that drive a mean flow seaward if the bay water levels are elevated. Under these conditions, inundated low-lying barriers effectively become submerged bars where wave-driven transport rates decrease with increasing water depth, and where cross-barrier water-level slopes control the sediment transport rate [*Donnelly et al*., 2006a].

1.2. Storm Surge Ebb

Hayes [1967] coined the term "storm surge ebb" for the bay-to-ocean flow that sometimes occurs during the waning stages of the storm, when offshore winds combine to set up bay water levels and set down ocean water levels, creating gradients that drive flow out of tidal inlets and newly formed breaches. *Hayes* [1967] speculated that these flows were responsible for generating density currents that deposited sand in relatively deep water (18 m) on the inner Texas shelf after Hurricane Carla (1961), and spread finer sediment even farther offshore. *Thieler and Bush* [1991] and *Lennon* [1991] noted extensive scouring of overwash channels by storm surge ebb in South Carolina during Hurricane Hugo (1989), which also transported sand offshore to depths of 7 m [*Birkemeier et al*., 1991; *Gayes*, 1991]. *Thieler et al*. [1989] documented severe erosion on the Yucatan Peninsula caused by storm surge ebb during Hurricane Gilbert (1988). Channels and small ebb delta lobes on the seaward side of Highland Beach in western Florida were created by storm surge ebb during Hurricane Andrew (1992) [*Tedesco et al*., 1995], and storm surge ebb produced seaward transport of sediment on the flanks of the Houston Ship Channel during Hurricane Ike (2008) [*Goff et al*., 2010]. Numerical hydrodynamic models of Hurricane Ivan (2004) demonstrated that large, offshore-sloping gradients in sea surface elevation, which could drive storm surge ebb, can develop behind Louisiana and Mississippi Gulf Coast islands following hurricane passage [*Sheng et al*., 2010] but the geomorphic impacts of these gradients were not explored. *Kahn* [1986] has described how storm surge ebb has resulted in subtidal sand deposits on the ocean side of the Chandeleur Islands and argued that the availability of this sand supply in the nearshore speeds poststorm morphologic recovery.

Seaward sloping water levels and seaward flow have been observed and modeled in other barrier island settings [*Pierce*, 1970; *Zecchetto et al*., 1997; *Peng et al*., 2004; *Rego and Li*, 2010]. They can result from several mechanisms, including freshwater discharge, wave-driven seawater flux into the bay, downwelling-favorable winds, tidal phase lags, and/or differences in amplitude or timing of water-level response to atmospheric pressure, winds, surge, or propagation of coastal-trapped waves. Elevated back-barrier water levels caused by freshwater discharge can generate seasonally ephemeral inlets in the glacier-fed hapua systems of New Zealand [*Hart*, 2009] and in river-mouth lagoons of, for example, California [*Kraus et al*., 2002], South Africa [*Cooper*, 2001], and Australia

[*Ranasinghe et al*., 1999; *Roy et al*., 2001; *Chewen et al*., 2009]. Groundwater flow can also increase water levels in, for example, small New England lagoons like Cards Pond, Rhode Island [*Cheung et al*., 2007]. Wave-induced flow, as overwash or across shallow inlets, also can elevate lagoon water levels [*Laudier et al*., 2011; *Olabarrieta et al*., 2011]. Numerical models of storms in the Gulf of Mexico show that a combination of wind patterns, storm track, and coastal geometry can result in wind-driven storm surge that is higher behind the barrier islands than in the ocean. This phenomenon is evident in the hindcasts of *Sheng et al*. [2010] for Hurricane Ivan (2004) and the SLOSH model [*Jelesnianski et al*., 1992; *Glahn et al*., 2009] forecasts archived for Hurricane Isaac (2012; http://www.nws.noaa.gov/mdl/psurge/archive.php). Regardless of the mechanism that elevates back-barrier water levels above ocean water levels, the resulting sea surface slopes can generate seaward flow and sand transport through breaches.

Despite the viable mechanisms for driving seaward flow across barrier islands and the scattered observations of its geomorphic products, most studies have focused on the attack of waves and storm surge from the ocean side, so the importance of seaward transport processes in barrier island evolution is difficult to assess and may be underestimated. Back-barrier conditions that can generate storm surge ebb are not included in most models of wave overtopping and overwash [for example, *Donnelly et al*., 2009; *Park and Edge,* 2010; *Figlus et al*., 2011; see *Donnelly et al*., 2006a, 2006b]. Except for *Lindemer et al*. [2010], there have been few attempts to model three-dimensional geomorphic evolution during inundation events and none where the models have benefited from prestorm and poststorm observations and measurements of physical processes during the event. Relationships developed between morphologic change and storm intensity rely mostly on subaerial features, especially overwash deposits [for example, *Morton and Sallenger,* 2003; *Carruthers et al*., 2013], and although the cut and fill signatures of channels appear in barrier island stratigraphy [*Buynevich and Donnelly*, 2006], sequences of overwash deposits are the principal stratigraphic proxies used to reconstruct storm records [for example, *Emery,* 1969; *Donnelly et al*., 2001a, 2001b, 2004a, 2004b; *Cheung et al*., 2007]. Ocean-side deposits produced in a major storm may be ephemeral and have no subaerial expression and are not recorded in the overwash stratigraphy. Thus, the events that generate seaward transport may be underrepresented in reconstructed records, conceptual models, numerical models, and field observations.

1.3. Objectives

The objectives of our study were to measure waves and water-level slopes during an overwash/inundation event and, with the aid of a numerical model, relate those forcing mechanisms with geomorphic changes determined from photos and topographic measurements made before and after the events. We are not aware of any measurements of water levels across a barrier island during inundation, so we chose to make measurements on the Chandeleur Islands during hurricane season, where the combination of low elevations and the remnants of an artificial berm increased our chances of observing conditions that produced significant morphological change. We anticipated measuring landward water surface slopes that, in conjunction with waves, would drive landward transport and form overwash deposits. We were able to record waves and water levels over the course Hurricane Isaac, a category 1 hurricane, including the initial overwash and eventual inundation of the barrier island, but our observations and model results, which showed seaward transport, were unexpected. The objectives of this paper are to present our direct measurements of waves and water levels, and detailed measurements of barrier island topography before and after Hurricane Isaac, and to discuss results of model simulations based both on the observed conditions and on alternative water-level scenarios. The model results demonstrate the profound influence of cross-barrier water-level variations in determining transport direction and geomorphic response, so our final objective is to discuss the broader implications of these results for other barrier systems.

2. Observations

2.1. Study Site

The Chandeleur Islands (Figure 1) are a long, low-lying (maximum elevation < 2 m) arc of sandy, partially vegetated islands perched on the remnants of the abandoned St. Bernard lobe of the Mississippi Delta. They were formed from deltaic deposits reworked by waves into paired flanking barrier spits [*Penland et al*., 1985; *Otvos*, 1986; *Twichell et al*., 2009, 2013], but the exact nature of island genesis has been debated [*Otvos and Carter*, 2013]. The abandoned lobe is subsiding from soil compaction [*Penland and Ramsey*, 1990], tectonic movement [*Dokka et al*., 2006], and possibly from oil and gas extraction [*Morton et al*., 2002]. Tropical cyclones are the primary agents of geomorphic change [*Hayes*, 1967], but the islands are subject to waves

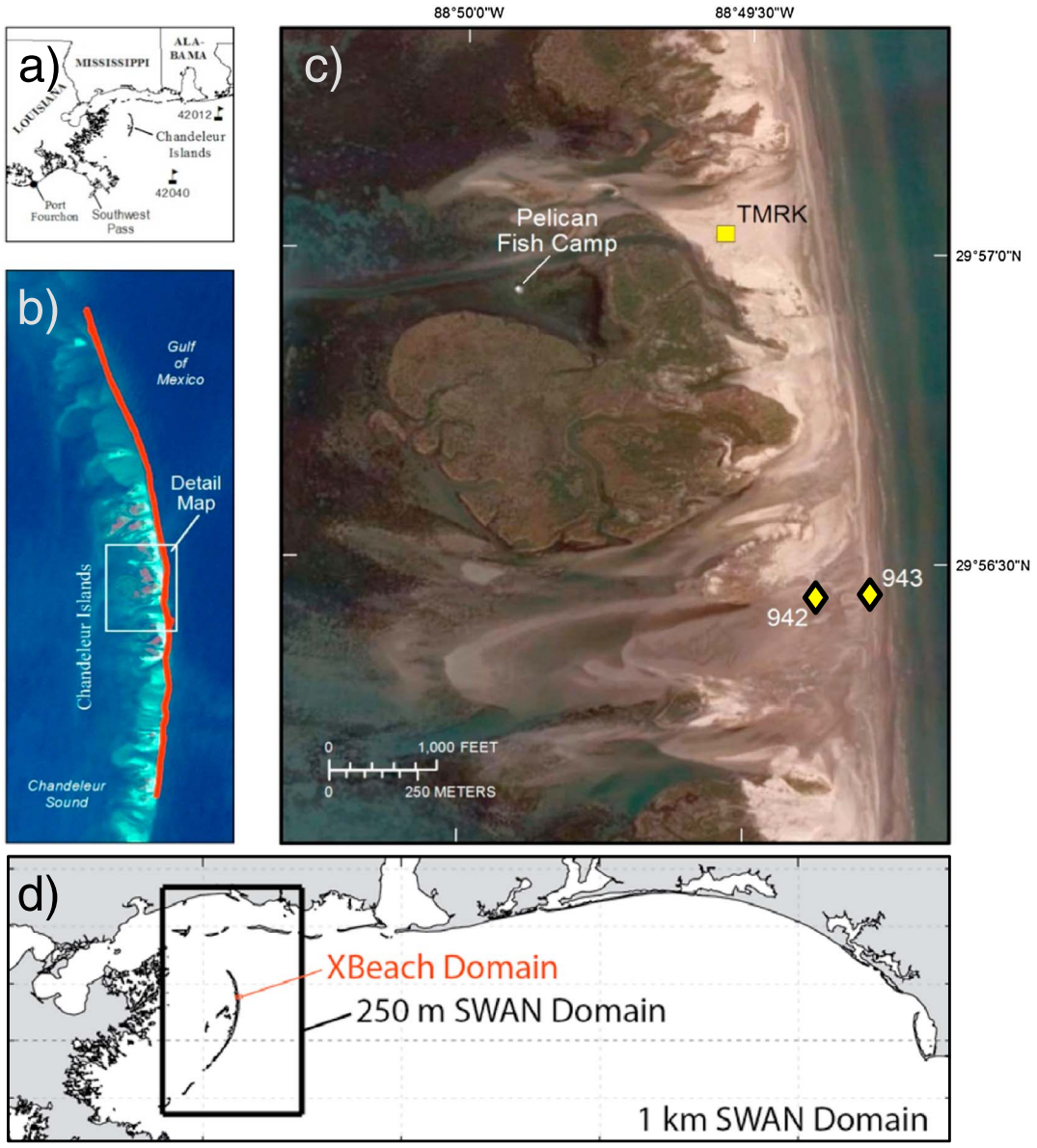

Figure 1. (a) Location map of the Chandeleur Islands in the northeastern Gulf of Mexico. (b) U.S. Geological Survey Landsat 5 image of the Chandeleur Islands, 18 February 2010, overlaid with a red line indicating the location of the artificial berm [*Plant and Guy*, 2013a, 2013b]. (c) Aerial photo of the study site on the northern Chandeleur Islands 2 months after Hurricane Isaac showing the locations of the Pelican fishing camp (white dot), the USGS benchmark TMRK (yellow square), and the water-level wellsites 942 (bay side) and 943 (ocean side, both yellow diamonds). Google Earth image dated 29 October 2012 © 2013 Terrametrics. (d) Map of the numerical model domains. Wave boundary conditions were provided to the XBeach morphology model by the 250 m SWAN wave model, which in turn was nested into a 1 km SWAN model. Boundary conditions for the 1 km SWAN were provided by a WAVEWATCHIII® model discussed in the text.

and surges associated with winter cold fronts that can rework the littoral zone. There is no alongshore or fluvial source for sand in the Chandeleurs, and the littoral sand supply is exchanged between the shoreface, nearshore, and inner shelf. The Chandeleurs are generally thought to be in the late part of the second stage of a three-stage sequence of evolution [*Penland et al.*, 1985] from (1) sand spits flanking the remnants of a reworked distributary lobe to (2) an island chain separated from the retreating mainland to (3) submerged shelf shoals. *Fearnley et al.* [2009] have documented ongoing fragmentation of the barrier arc into series of small islands and submerged bars, with associated loss of supratidal area, and very little transgression of back-barrier deposits and marsh.

Our study builds on a long history of observations of geomorphic evolution of the Chandeleurs that began with U.S. Coast and Geodetic Survey maps in 1855 [*McBride et al*., 1992] and led to recent oblique aerial photography, satellite, and lidar surveys conducted along with geophysical surveys and field studies led by the U.S. Geological Survey (USGS) [*Fearnley et al*., 2009; *Lavoie*, 2009]. An artificial berm was constructed on the Chandeleur Islands beginning in June 2010 as part of the response to the Deepwater Horizon oil spill [*Louisiana Department of Natural Resources*, 2010]. Construction continued through April 2011. Because berms are one of the methods used to nourish beaches on barrier islands, this project on an undeveloped island with little human activity served as a large-scale experiment in morphologic response to artificial berms [*Lavoie et al*., 2010; *Plant et al*., 2014]. The Chandeleur Islands are a good location for measuring overwash because of their low elevation. They also provide a good location for testing models of storm-induced morphological change because island geometry is relatively simple, with uniform sand size, large regions with little vegetation, no development, and very little human alteration. The artificial berm built on these low-lying islands was likely to undergo significant geomorphic change and provided an opportunity to observe these processes. We chose the specific location of our instruments to maximize the probability of observing overwash by placing them on either side of a low point in the remnants of the artificial berm in a region historically and episodically occupied by an overwash channel observed in satellite and aerial photographic images.

2.2. The Storm

Hurricane Isaac made the first of two landfalls near Southwest Pass on the southeast Louisiana coast at 0000 UT on 29 August 2012 as a category 1 hurricane with maximum sustained winds of 36 m/s [*Berg*, 2012]. The center of the storm drifted offshore toward the south and west, and it made a second landfall west of Port Fourchon, Louisiana, at 0800 UT on 29 August. The slow movement resulted in more than 25 cm of rain, storm surge of up to 3.4 m in southeastern Louisiana, and inland flooding in southeastern Louisiana and southern Mississippi and Alabama. The combination of storm surge and wind was sufficient to reverse the flow of the Mississippi River at Belle Chasse, Louisiana, for more than 13 h on the night of 28–29 August (http://waterdata.usgs.gov/usa/nwis/uv?07374525). The trajectory and speed of the storm, wind patterns, and coastal geometry generated water levels that were higher in Chandeleur Sound than they were in the Gulf of Mexico for an extended portion of the storm. The National Oceanic and Atmospheric Administration (NOAA) probabilistic storm surge forecast showed a progression of water-level increases and a change in the water-level slope from onshore sloping (advisory 26, on 27 August 2012), to offshore sloping (advisory 29, 28 August 2012 through advisory 35 on 29 August 2012). The analysis of *Keim et al*. [2007] suggests that the return interval for a storm of this intensity is 3–8 years.

There were few wave measurements in the eastern Gulf of Mexico during Isaac, as the closest National Data Buoy Center buoys were out of service. Buoy 42012, located 80 km southeast of Mobile, Alabama, and 120 km east of the Chandeleurs, recorded maximum significant wave heights of 5.78 m with dominant periods of 12–13 s at 2100 on 28 August. Our estimates from wave models (see below) indicated that wave heights at the location of buoy 42040 (Figure 1) peaked at 9.6 m 5 h earlier than peak waves at 42012. Closer to the Chandeleur Islands (at the 8 m contour, where they were used as offshore boundary conditions for the XBeach geomorphic model discussed below) modeled waves peaked at 3.3 m, with a maximum period of 13 s from the south-southwest.

2.3. In Situ Water-Level Recorders

Water levels were measured on either side of the barrier beach (Figures 2 and 3a) in an inactive overwash channel. Instantaneous measurements were made every 5 s with autonomously recording temperature-compensated pressure loggers (RBR Inc. model DR 1060, 10 m operational depth) in two shallow wells installed 143 m apart on opposite sides of the island. At the time of installation on 10 July 2012, these wells straddled a low spot in a continuous subaerial island crest trending north–south (Figure 2c). This crest was the remnant of an artificial sand berm built in the autumn of 2011 [*Plant and Guy*, 2013a, 2013b]. Although there was evidence of previous overwash (a broad dry channel with ripple marks leading to an accretionary lobe on the west side), wrack and small aeolian features suggested that the crest had been dry during recent high tides. The wells were installed at low tide near the waters' edge by digging shallow holes (about 0.4 m deep; these immediately filled with groundwater) and using a battery-powered bilge pump to jet 4.8 cm (outside diameter) schedule 80 PVC casings to depths of about 1.5 m. The pressure sensors were hung from threaded well caps at fixed elevations on stainless-steel rods, and the elevations of the well caps were

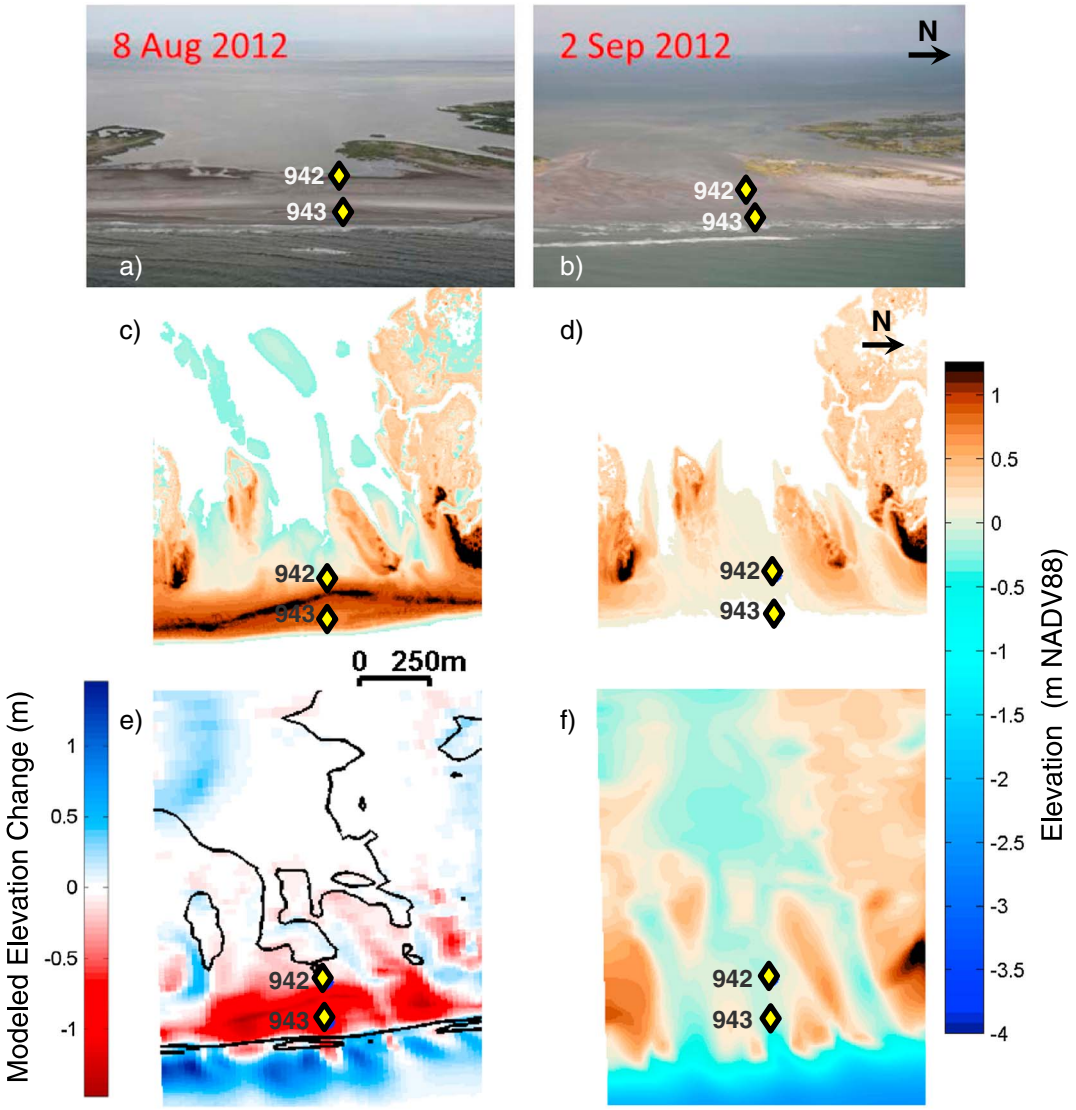

Figure 2. (a) Oblique photo of the instrument deployment area 20 days before and (b) 2 days after Hurricane Isaac. Approximate instrument locations are indicated by yellow diamonds in all panels. (c) Lidar measured topographic elevations obtained 8 months before (6 February 2012) and (d) 10 days after Hurricane Isaac (10 September 2012). (e) Simulated elevation change with blue indicating modeled accretion and red indicating erosion. The solid black line denotes the prestorm 0 m elevation contour. (f) Simulated poststorm elevations, for comparison with Figure 2d. All elevations are referenced to North American Vertical Datum of 1988 (NAVD88).

surveyed with differential GPS. The well casings were permeable with narrow (0.15 mm) slits along most of their length, and there was a 1.25 cm diameter hole (used for jetting) in the conical well point at the bottom of each casing. The wells were recovered on 7 September 2012, 8 days after Hurricane Isaac. A second pair of wells, installed on either side of the barrier approximately 5 km north of the wells described here, was lost during the storm. Atmospheric pressure measurements were made at 10 min intervals with an Onset Hobo model U20 mounted about 4 m above water level on a radio tower at the north end of the Chandeleur Islands, about 13 km from the study site.

We used these measurements to make precise estimates of water levels and water-level slopes at the cross-island transect. The specified accuracy of the pressure loggers was 0.05% of full operating depth, or about 0.5 cm water depth. Rated resolution was 0.001% of full scale (0.01 cm). Field calibrations in a bucket before and after the experiment confirmed that the two sensors had not drifted, and agreed within <0.01 dbar (<1 cm water depth). Atmospheric pressure measurements (linearly interpolated in time) were subtracted

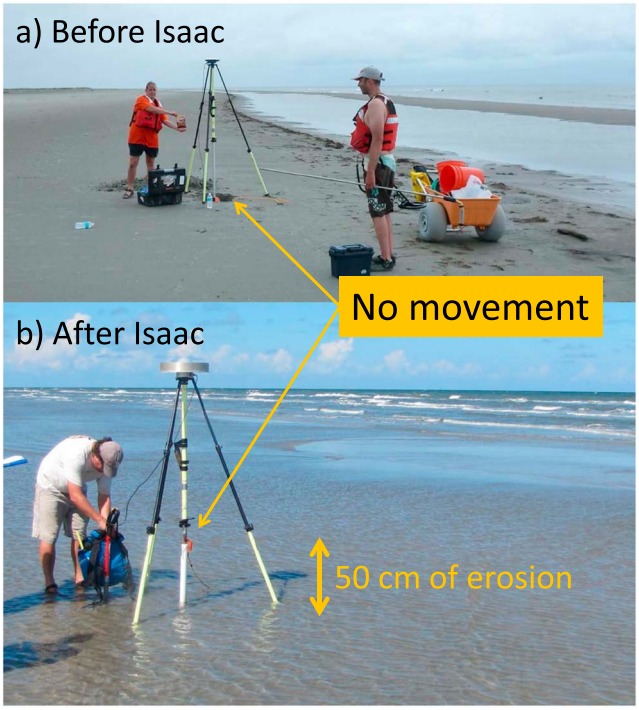

Figure 3. (a) Nancy DeWitt and Pat Dickhudt getting a GPS fix on the ocean side (Gulf of Mexico, site 943) well after installation on 10 July 2012. The well casing is below beach level and only the orange tag on the cap is visible. (b) B.J. Reynolds getting a GPS fix on the same well on 7 August 2012 after Hurricane Isaac. The white well casing extended a half meter above the sand and the GPS data verified that it had not moved, so more than 50 cm of sand was eroded from this site during the storm.

from the well pressure measurements p (decibars), which were then converted to water depth η (m) according to $\eta = 10^4 p/(\rho g)$, where ρ is typical water density (1023 kg/m^3), g is gravitational acceleration (9.81 m/s^2), and the dimensional factor 10^4 Pa/dbar is a unit conversion. Water-level time series $\overline{\eta}(t)$ were calculated using a running mean over 5.7 min intervals ($N = 241$ samples). The 95% confidence intervals (δ_η) about $\overline{\eta}$ were estimated from the standard deviations of the means [*Bendat and Piersol*, 1986, p. 433]. δ_η varied with wave height and rate of water-level change, with maximum values of 2.1 cm at the bay site and 2.3 cm at the ocean site. The time series of water-level slopes $s(t)$ was calculated as $s = \left(\overline{\eta}_{\text{ocean}} - \overline{\eta}_{\text{bay}}\right)/L$, where $L = 143.37$ m was the distance separating the wells. Analysis of uncertainties about $\overline{\eta}$ considered instrument accuracy (±1 cm), surveying error (±0.5 cm), possible movement of the wells (maximum 2.4 cm), and time series of δ_η (which ranged from $<$0.1 to 2.3 cm). It did not account for errors associated with removal of the atmospheric pressure or conversion from pressure to water depth, because these were small and data from both wells was affected equally. Propagation of the uncorrelated uncertainties [*Taylor*, 1997] suggests that our worst case error in absolute water-level elevations for 5.7 min averages was ±3.4 cm. Assuming that δ_η at each of the wells was uncorrelated, uncertainties in water-level slopes were ±0.0003.

Water levels in shallow wells respond to the water table in the beach, which is controlled by island elevation and seawater elevations, and modified by rainfall and evaporation [*Emery and Foster*, 1948; *Horn*, 2002]. Before the storm, when the gauges were in the intertidal zone, our measurements were consistent with previous observations [*Nielsen*, 1990, 1999]: the water table was elevated above the low-tide level and rose faster than it fell over a tidal cycle, lagging the observed tides. In addition, the water table on the ocean side was higher than the water table on the bay side, a phenomenon called overheight, caused by wave setup and infiltration of swash runup [*Waddell*, 1976; *Kang et al.*, 1994; *Li et al.*, 1997]. There were episodic spikes in water elevation that we attributed to infiltration of rainwater. However, in this paper we focus on the time during the storm when the wells were completely submerged, and the only significant difference between our measurements with pressure sensors buried in sand and those more commonly made by pressure gauges in the water column was increased damping of the response at higher frequencies. We used the method of *Raubenheimer et al.* [1998] to estimate a frequency-dependent correction factor for the overlying sand that varied with time as water depth and the pressure-sensor burial depth changed. We have measurements of the sensor burial depth at deployment and recovery, and we assumed it decreased linearly during the storm. The correction factor ranged from about 1.4 at the highest frequency (0.1 Hz), to about 1.04 at 0.05 Hz (period of 20 s), which we used as the low-frequency limit for incident-wave energy, to close to 1 (no correction) at lower frequencies.

Root-mean-square (RMS) wave heights were calculated from the water-level data as $2\sqrt{2}$ times the square root of the corrected spectral variance of water surface elevations in the incident ($f \geq 0.05$ Hz) and infragravity bands ($0.0037 \leq f < 0.05$ Hz). These estimates were not sensitive to the attenuation correction factors

discussed above, or to our uncertainty in water depths, which together caused variations of <6% in our estimates of RMS wave heights.

2.4. Lidar Topography

Lidar topography was collected on 6 February 2012, 7 months before Hurricane Isaac. The lidar data were processed to bare-earth classifications to remove influences of vegetation and the elevations were compared to ground survey data. The data were corrected to the ground survey data, and the resulting, corrected data had errors (standard deviation) of less than 0.10 m [*Guy et al*., 2013]. Gridded data (Figure 2c) near our water-level gages show the remnant of the artificial berm constructed in November 2010. The berm crest near our site was about 1.4 m NAVD88, with low spots only 0.9 m high. Our field observations suggest that much of this berm was reworked by the time we deployed our gages on 10 July (Figure 2a). The highest point anywhere on the northern Chandeleur Islands in the gridded February lidar survey was 1.67 m NAVD88, located in the marshy island north of our gages. Estimates from the NOAA VDatum tidal model and comparison with datum from tide gauges on the Mississippi coast indicate that the mean water level at the Chandeleur Islands is 0.16 m NAVD88, so the highest point on the islands was 1.51 m above mean sea level (msl).

A second set of lidar topographic elevations was collected after Hurricane Isaac on 10 September 2012 and processed in the same manner. These data show a general lowering of island elevations and relocation of sand, removing any subaerial evidence of the remaining artificial berm (Figure 2c, http://coastal.er.usgs.gov/hurricanes/isaac/lidar/). Elevations near the instruments (<200 m away) were reduced to less than 0.2 m NAVD88, and channels connecting the ocean and bay were incised in numerous locations.

2.5. Sediment Samples

We collected samples of the top 2 cm of sediment at both sites and analyzed those using sieve and sedigraph methods [*Poppe et al*., 2005]. The beach on the ocean side consisted of clean fine sand (median 0.15 mm, <1% silt + clay). On the bay side we found very fine sand (0.11 mm) with a larger silt component (2% silt + clay).

3. Model Description and Application

Quantitative observations of geomorphic change during dune and barrier island overwash and inundation do not exist aside from laboratory experiments [e.g., *Figlus et al*., 2011], but numerical models provide a mechanism to simulate island evolution driven by these processes. Here we used the hydrodynamic observations at the two locations across the barrier island to constrain the bay and ocean model boundary conditions and examine the sensitivity of geomorphic evolution to the magnitude and direction of the water-level gradients observed during Hurricane Isaac. These gradients are not typically measured on these spatial or temporal scales during storms, but the observations of breaching and channel deepening caused by storm surge ebb demonstrate their importance for geomorphic change.

We used XBeach (repository version 2970), a process-based model developed to simulate storm-induced beach and dune evolution [*Roelvink et al*., 2009]. XBeach has been used to successfully simulate retreat of a dune face caused by elevated water levels colliding with the dune [*Splinter and Palmsten*, 2012] and overwash-induced lowering and breaching of Santa Rosa Island, Florida, during Hurricane Ivan [*McCall et al*., 2010]. The two-dimensional depth-averaged model described in detail by *Roelvink et al*. [2009] simulates wave-averaged incident waves, circulation, sediment transport, and morphology evolution. XBeach resolves infragravity waves, which allows water levels to vary on the shoreface (e.g., infragravity wave runup), where a dune-avalanching algorithm is employed to model coastal erosion when waves collide with the dune face. During overwash events, wave groups are responsible for the landward flux of momentum that lowers dune elevations and transports sediment onshore. Sediment concentration and transport is governed by a depth-averaged advection-diffusion equation [*Galappatti and Vreugdenhil*, 1985] where increases or decreases in sediment concentration within the water column are dictated by an equilibrium sediment concentration [*Soulsby*, 1997].

We applied XBeach to a 1.5 km central section of the Chandeleur Islands for the time period 27 to 30 August 2012. Model resolution in the alongshore direction was 20 m, and the domain extended east toward the Gulf of Mexico to a water depth of approximately 8 m with a cross-shore grid resolution that varied from 40 m offshore to 2.5 m in the surf zone and across the island and about 1 km west to back-bay water depths of approximately 1.5 m. Most of the domain, except for the seaward portion extending to 8 m depth, is shown in Figure 2. Various data sets were used to construct the bathymetry for the model grid including data obtained

from the NOAA National Geophysical Data Center Northern Gulf Coast digital elevation map and USGS single beam and swath bathymetry measurements collected in 2006, 2010, and 2011. Topographic data from the February 2012 lidar survey were used to define the island elevations. All of the data were merged into a single grid using the scale-controlled interpolation method of *Plant et al.* [2002] with the most recent data more highly weighted.

Wave boundary conditions on the eastern (ocean) side of the XBeach model were hourly wave spectra with an assumed Joint North Sea Wave Project (JONSWAP) shape [*Hasselmann et al.*, 1973]. Radiation conditions for waves were applied at the other three boundaries. The JONSWAP spectra were generated from wave statistics (significant wave height, peak period, and direction) produced by a Simulating Waves Nearshore (SWAN) wave model [*Ris et al.*, 1999] run on a 250 m grid (Figure 1d). Boundary conditions for this model were time-varying 2-D wave spectra from a 1 km SWAN model (Figure 1d), which was one-way nested onto a larger-scale WAVEWATCHIII® (WW3; version 3.14 [*Tolman,* 2008]) wave model system (not illustrated) with a sequence of three two-way nested domains. The WW3 domains consisted of a 30′ global grid and a 10α′ western north Atlantic grid, identical to those used by the operational NOAA wave forecasting system (http://polar.ncep.noaa.gov/waves/index2.shtml). The finest WW3 domain, which provided boundary conditions for the 1 km SWAN grid, was a 2′ Gulf of Mexico grid derived from the ETOPO1 Global Relief Model (http://www.ngdc.noaa.gov/mgg/global/global.html). The wave model system was spun up over the period of 1 to 27 August 2012. Wind (and ice) forcing files for all models were derived at 3-hourly resolution from archived 12 km NOAA North American Mesocale model forecasts over its domain and otherwise from the 28 km Global Forecasting System. Although there were no data for evaluation of the high-resolution (250 m grid) SWAN wave model at our study site, model-data comparison of significant wave heights at buoy 42012 produced a correlation of $r^2 = 0.984$ and bias of 7.4 cm.

Water-level boundary conditions for XBeach along the bay and ocean boundaries were derived from the buried-pressure-sensor measurements. Flow conditions at these boundaries allowed for automatic adjustment to the water-level forcing, and zero-gradient (Neumann) conditions [*Roelvink et al.*, 2009] were applied along the lateral (north and south) boundaries. The observed water levels included contributions from astronomical tides, storm surge, setup induced by wave breaking, and wave runup. XBeach simulated the latter two components, so they had to be removed from the measurements before using them as boundary conditions. Wave runup was removed by low-pass filtering the water-level time series with a cutoff period of 20 min. Wave setup was removed by subtracting elevations that were calculated using a one-dimensional cross-shore balance between sea surface slope and the gradient of momentum flux (onshore component of radiation stress) following *Thornton and Guza* [1983] with *Stoker*'s [1957] formula for dissipation in a bore. Wave setup was assumed negligible on the bay side of the island and was not removed from the observations. Removing wave-induced setup from the ocean-side observations reduced water levels used as boundary conditions for XBeach by 15–25% during the course of the storm.

4. Results

4.1. Elevation Changes

A significant amount of sand was removed during Hurricane Isaac. When the instruments were installed on 10 July 2012, the well caps were slightly below grade, covered with 0.02–0.05 m of sand (Figure 3a). When the instruments were recovered 8 days after Hurricane Isaac, the wells were found standing proud 0.28–0.52 m above the surrounding sand and survey measurements confirmed that the wells had not moved (Figure 3b). Sand levels decreased by 0.54 m on the ocean side and 0.30 m on the bay side, and the berm crest that initially separated them was gone, suggesting that a minimum of 60 m^3/m was removed between our wells.

4.2. Mean Water Levels and Gradients

Water levels fluctuated with tides and winds before Hurricane Isaac, and the water-level recorders measured groundwater response to these fluctuations (Figure 4). Before Hurricane Isaac, the mean water elevation on the bay side was 0.26 m NAVD88, and on the ocean side was 0.33 m NAVD88, compared with our long-term estimated mean water level of 0.16 m NAVD88. These are consistent with observed water levels 65 km away at Waveland, Mississippi, in late August, which were typically ~0.15 m (ranging from 0.05 to 0.35 m) above predicted tides.

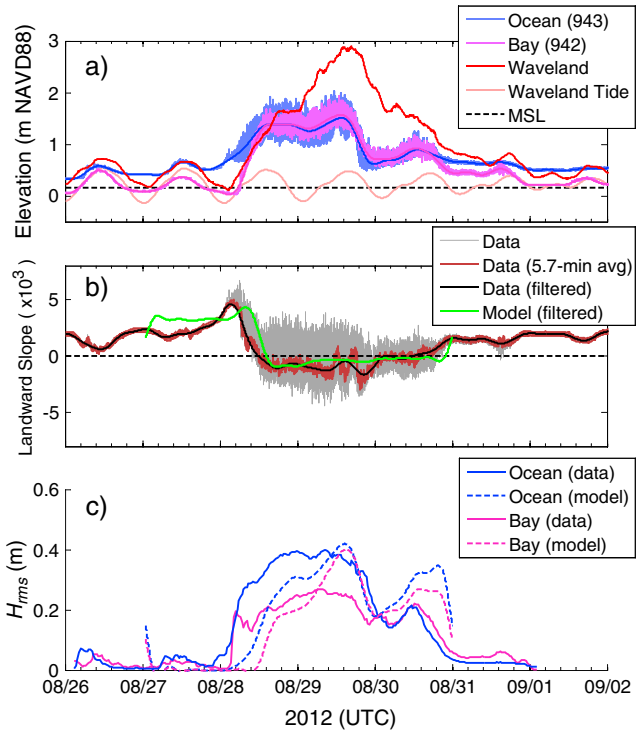

Figure 4. (a) Time series of water levels from the wells on the ocean (Gulf of Mexico) and bay (Chandeleur Sound) sides of the Chandeleur Islands, along with measured water levels at the Bay Waveland Yacht Club on the Mississippi Coast, about 60 km NW of the Chandeleurs, and predicted tides at that location. (b) Sea surface slopes between the wellsites. Measured instantaneous (gray), envelope of $\pm\delta\eta$ around 5.7 min running mean (brown), and low-pass filtered (black) slopes, and modeled low-pass filtered (green) slopes. (c) Root-mean-squared (rms) wave heights estimated from the water-level spectra at the two wells (solid) and modeled rms wave heights at the same locations (dashed).

The sequence of events during Hurricane Isaac was as follows. Water levels rose first on the ocean side of the barrier as the storm approached (Figure 4a), and water-level variations caused by waves first appeared about 0400 UT on 28 August (Figure 4c). At this time, the water levels on the ocean side were nearly a meter higher than on the bay side, as indicated by the peak in the slope (Figure 4b), and overwash was likely occurring in the form of swash runup. Water levels started rising on the bay side soon afterward (around 0500) and the water surface slope began to decrease, indicating a hydraulic connection between the two sites. By 1430, water levels on both sides were nearly equal at about 1.4 m NAVD88 and the slope decreased to zero. At these water elevations, the berm crest between our sites would have been inundated, and broken waves would have been crossing the island. The storm continued to intensify, and RMS wave heights peaked on the seaward side at about 0.37 m around 2300 UT on 28 August. Starting at midnight UT, water levels began to fall slightly with ebb tide, and the cross-barrier slope began to tilt slightly toward the ocean. Wave heights on the bay side continued to increase after they had peaked on the ocean side, which indicates that less wave energy was being dissipated across the island, possibly because the overwash channel was eroding and deepening. Highest waves on the bay side reached about 0.25 m. The wave height/water depth ratio was consistent with broken waves on the ocean side, and the waves on the bay side were likely broken bores that propagated across the barrier. The highest water levels coincided with high tide between 1400 and 1500 on 29 August. Water slopes were tilted slightly seaward (typically -0.0005 ± 0.0003, but as much as -0.0009 ± 0.0003 m/m) for all day on 29 August.

Maximum instantaneous water levels at the peak of the storm (including waves) were 1.94 and 2.03 m NAVD88 on the bay and ocean sides, respectively, exceeding the highest point on the island by 0.27–0.36 m. Maximum 5.7 min running-average water levels were 1.46 and 1.44 m NAVD88, respectively, highest on the bay side (Figure 4a).

The bottom shear stress τ_b associated with observed seaward slopes $s(t)$ of about 0.0005 m/m were estimated as $\tau_b = \rho g h s$, where $h(t)$ is time-varying water depth. Reverse calculations indicate that water depth of about 0.32 m is required for these slopes to mobilize 0.15 mm sand, assuming a critical shear stress of 1.6 Pa (based on *Soulsby* [1997]). Even without channelization, these depths were exceeded for most of the storm, and with addition of wave-induced stresses, these slopes should have generated significant sediment transport, as described in section 4.3.

4.3. Model Results

4.3.1. Hydrodynamics

The modeled water levels were output every 5 s, compared to observed water levels, and used to calculate the sea surface slopes (Figure 4b). Modeled water-level elevations closely matched observations

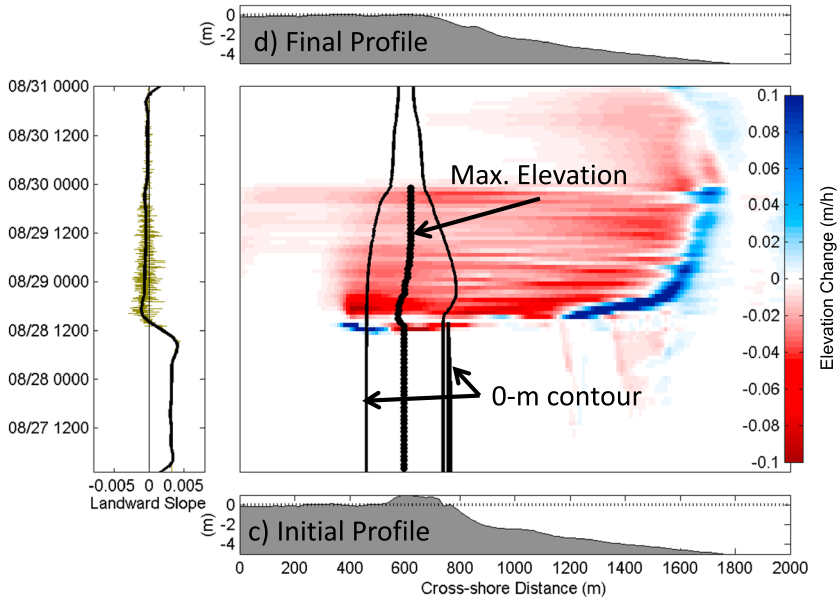

Figure 5. Simulated morphology change during Hurricane Isaac. (a) Instantaneous (yellow) and 20 min filtered (black) slope of the modeled cross-island water levels computed at the instrument locations. Landward slopes are positive and seaward slopes are negative. (b) Timestack of hourly elevation change at the cross-shore model transect closest to the instrument wells. Times are indicated in Figure 5a. Red and blue denote erosion and deposition, respectively. The dotted line is the time-varying cross-shore position of the island crest (maximum elevation) and the solid lines show the 0 m contours on the bay (left) and ocean (right) sides of the island. (c) Elevation profile used to initialize the model simulation before Hurricane Isaac. (d) Final simulated elevation profile after Hurricane Isaac.

(maximum 10 cm difference) after an initial period when the modeled waves (and therefore setup) ramped up later than observations.

Magnitudes of the modeled RMS wave heights were comparable to the observed heights, although the temporal variations were not identical (Figure 4c). The maximum wave height at the eastern instrument (ocean) was well represented, but the model overpredicted waves at the western (bay) instrument. The difference in wave heights on the two sides of the island was larger in the observations than in the model results, indicating the model may not have been dissipating enough wave energy when water levels were high and the island was completely inundated. Dissipation generated by depth-induced wave breaking would be underpredicted if the model was overpredicting erosion. However, there is uncertainty in the wave height observations, because they were determined, in part, by estimating the water depth.

4.3.2. Morphology

Modeled erosion during the ramp up of the storm was minor and confined mainly to the beach face, with deposition in the nearshore. When water levels on the Gulf side approached 1 m (1100 UT on 28 August) overwash began at low points in the artificial berm, causing erosion of the berm crest and landward sediment transport. As water levels continued to increase, landward sediment transport rates increased and a lowering of the entire berm was modeled until 1500 UT on 28 August, when erosion of the island continued, but the transport direction reversed. The modeled sediment was deposited in the nearshore despite large wave action on the ocean side. The model did not produce the landward oriented overwash fans usually associated with overwash and inundation events; instead, the model predicted a significant amount of sediment deposition on the ocean side of the island during times when the water-level gradient across the island was directed seaward.

Observed poststorm morphology showed that multiple channels connecting the ocean and bay had fragmented the island (Figure 2f). The modeled poststorm channelization occurred in the same areas (compare Figures 2d and 2f), but modeled elevations for the remaining subaerial island elevations were slightly lower than observed due to excessive smoothing by the model. The smooth results were caused, in part, by initializing the model with a homogeneous sand size and erodibility that neglected the presence of marsh vegetation and spatial variation in sediment types, including grain size and organic content. Although the channels appear deeper in the model results, a bathymetry survey was not conducted following the

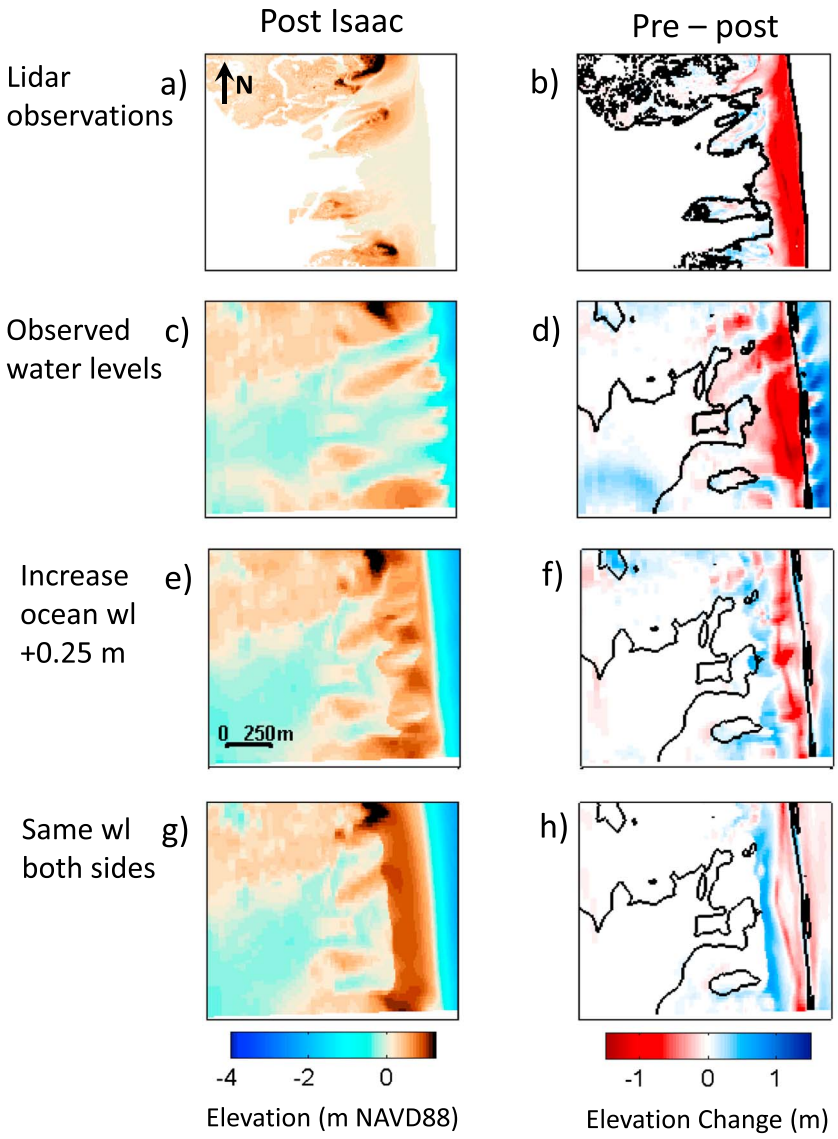

Figure 6. (a) Lidar topography observed September 2012 and (b) elevation change between February 2012 and September 2012. The thick black lines denote the prestorm 0 m topographic contour. Blue colors indicate accretion and red colors erosion. (c) Simulated poststorm island elevations for the base case with observed water levels (wl) minus runup and setup. (d) Simulated elevation change for the same simulation. (e) Simulated poststorm island elevations for sensitivity run 1 when model was initialized with offshore storm surge increased by 0.25 m. (f) Simulated elevation change for the same simulation.(g) Simulated poststorm island elevations for sensitivity run 2 when model was initialized on the bay and ocean with the same water levels. (h) Simulated elevation change for the same simulation. All elevations are referenced to North American Vertical Datum of 1988 (NAVD88).

storm and the lidar was incapable of measuring underwater features, so the interpolation of the lidar data results in approximately 0 m elevation across the channels.

Modeled results indicated that the mean offshore-directed cross-shore flows over the berm crest peaked at about 35 cm/s when the seaward water-level slope was at its maximum. On average, the mean cross-shore flows during the time when bay water levels exceeded the ocean water surface elevation were approximately 20 cm/s. Modeled elevation change (Figure 2e) suggested that sediment was transported in the seaward direction and deposited in the active littoral zone. This is counter to traditional barrier rollover where overwash fans develop on the low-energy back barrier system. The prestorm 0 cm elevation contour is shown in Figure 2e for reference. The transition from landward transport to deposition of sand on the ocean side can be seen in the timestack of

elevation change at the model transect closest to the instruments (Figure 5). At the beginning of the storm only mild change occurred, caused by waves colliding with the front of the island. Water levels were higher on the ocean side, but it was not until approximately 1200 UT on 28 August that modeled overwash began, causing erosion of the berm and landward deposition of sediment. This lasted only a few hours before the island was inundated and the connected water surface slope reversed, and transport was again directed seaward, causing erosion on the island and shoreface and deposition offshore between the 2 and 5 m isobaths.

4.4. Sensitivity to Water Levels

Two additional simulations were performed to investigate the sensitivity of modeled morphologic change to water levels. These involved changing the water-level boundary conditions (1) to increase the ocean side storm surge 25 cm higher than observed, thereby imposing landward-directed water-level gradients throughout the entire storm, and (2) to apply the same water level to both sides so that water-level gradients would be due only to differences in wave setup and runup. The poststorm morphology and changes resulting from these two simulations are shown in Figure 6.

The first sensitivity simulation demonstrated that when a water-level gradient existed but was directed landward, the total amount of island erosion was reduced and the majority of deposition occurred landward of the original island position (Figures 6a and 6b) as overwash deposits and fans. Channels were still evident but were much shallower than in the base case, indicating that the model was sensitive to the direction and magnitude of the water-level gradients. In the second sensitivity simulation, the island responded with further reduction in erosion and with more alongshore uniform overwash (Figures 6c and 6d) and no channels formed. More sediment was deposited on the landward side of the barrier compared to the other cases, and there was less deposition in the littoral zone, indicating that the contribution to sand transport by a mean cross-barrier flow is significant for the geomorphic response of a barrier island to a storm.

5. Discussion

5.1. Observations

Our observations may be relevant to other barrier island settings susceptible to inundation. There are many locations on the coasts of the Gulf of Mexico and western Atlantic where inundation is possible during extreme events [*Stockdon et al.*, 2012]. The northern Chandeleur Islands are more susceptible than most because their threshold for overwash is only about 1.42 m above msl [*Rosati and Stone*, 2009]. They occupy a subsiding delta and are experiencing rapid relative sea-level rise (approximately 4.3 mm/yr [*Twichell et al.*, 2013]), and they have no alongshore supply of sand. The artificial berm installed in 2010 created a modified topography that was rapidly and substantially altered by natural processes prior to, and during, our study period. Chandeleur Sound is not a typical lagoon, but rather a broad, shallow bay, open to the north and south, responsive to wind-driven water-level fluctuations, and perhaps more conducive for development of seaward directed water-level gradients. Despite, and in some instances because of these defining characteristics, the northern Chandeleur Islands are a valuable natural laboratory for developing and evaluating models because they allow us to observe rare, episodic phenomena more frequently than at other locations. Hence, our measurements provided unique observations of processes that occur on portions of most barrier beaches but are too infrequent to easily observe.

One shortcoming of our observations was the 7 month time period between the prestorm lidar survey and landfall of Isaac. We inspected satellite imagery and model predictions of overwash [*Plant et al.*, 2014] and determined that there were at least two overwash events that modified the topography between the February survey and August landfall. These events reduced the height of the remnant berm at the location where the water-level sensors were deployed. This depression was specifically selected for deployment to maximize overwash likelihood. Although it would be ideal to have immediate prestorm topography to initiate the model, it is possible that the simulated overwash quickly modified the topography to be consistent with pre-Isaac conditions (Figure 5) before the bay-to-ocean water-level gradient reversed the flow and sediment transport.

5.2. Model Results

Our baseline model simulation indicated that during Hurricane Isaac, higher water levels observed on the bay side resulted in significant sediment transport toward the ocean side, a process counter to traditional barrier rollover where large storms drive wave runup and overwash fans develop on the low-energy back barrier.

Two-dimensional simulations of inundated barriers have been compared with poststorm profiles [for example, *Donnelly et al*., 2006b; *Cañizares and Irish,* 2008], but previous models of barrier island response have not inspected in detail the three-dimensional geomorphic changes associated with seaward flow during inundation. Sensitivity of XBeach results to water-level variations in two-dimensional simulations of overwash during Hurricane Ivan on Santa Rosa Island, Florida, was investigated by *McCall et al*. [2010]. They found that the amount of deposition on the back barrier was sensitive to bay water elevations and the timing of bay- and ocean-side surges and noted that "the assumption of identical offshore and bay surge levels may not be correct" [*McCall et al*., 2010, pp. 678–679]. *Lindemer et al*. [2010] used a process-based numerical model (XBeach, the model used here) to perform simulations of Hurricane Katrina and found that although the model produced patterns of erosion and deposition similar to those observed, the amount of erosion was underpredicted. Their simulations were also hindered by lack of prestorm bathymetry, and they did not investigate cross-barrier storm-induced water-level variations which, as shown here, are capable of increasing island erosion due to a mean flow. Hence, *Lindemer et al*. [2010] could not identify the specific processes that produced morphologic change in the Chandeleur Islands during Hurricane Katrina.

The XBeach simulations reported here provide some of the first model results of geomorphic response to seaward flow during inundation. The model reproduced the channel incision observed in previous field studies and generated deposits in the shallow nearshore region that would not have appeared in poststorm subaerial topography. The model indicated a different geomorphic response when run without cross-barrier water-level gradients (an initial condition often applied in numerical models when observational data are lacking): in these cases, there was a more uniform geomorphic response with no channelization. The difference in geomorphic response between landward and seaward sloping water levels during storms is similar to the contrast between flood- and ebb-dominated features on mesotidal and microtidal tidal inlets [*Hayes*, 1975; *Boothroyd et al*., 1985].

5.3. Observational Bias?

Paradigms for the morphological evolution of barrier islands have been developed with a huge amount of subaerial observational data and relatively little submarine or subsurface data. Aerial photos, satellite images, and even lidar maps are cheap and plentiful, compared with acoustic bathymetric data, subbottom acoustic profiles, and ground-penetrating radar (GPR) lines. The nearshore region below low tide to ~10 m depths is particularly difficult to map, because turbid water limits photography and bathymetric lidar, saline groundwater inhibits GPR, and shallow depths are problematic for subbottom acoustical systems and decrease the efficiency of swath bathymetric data collection. Technology is improving our ability to observe bathymetric changes in the nearshore (for example, time-lapse photos can map bar locations and radar- and lidar-based measurements of wave heights can be used to infer bathymetry). However, we suggest that most of the information we have regarding the morphological impacts of severe and infrequent events has been developed through subaerial observations and that this is an observational bias that may lead to underestimates of the frequency and magnitude of upper shoreface deposits associated with seaward cross-barrier transport.

Overwash fans and flood-tidal delta deposits provide irrefutable and photogenic evidence of landward transport. Comparable evidence for seaward transport to the upper shoreface is less easily acquired, particularly on wave-dominated coasts. Thus, the role of seaward cross-barrier transport and deposition, even temporarily, in the nearshore regions may need to be considered in morphologic models. Clearly, landward transport must prevail for successful transgression. But not all barrier islands are rolling over.

5.4. Broader Implications

Model simulations demonstrated that net onshore transport does not necessarily increase monotonically with increasing storm surge and inundation depths, as was suggested in previous work [*Sallenger*, 2000]. We have already discussed the effect of reversing the water-level gradient. Additionally, increasing the inundation depth reduces the wave-induced bottom stresses, other things being equal. One implication of our observations is that for barrier island evolution, the largest storms may not be as effective at generating rollover and sequestering sand in overwash deposits as storms that are just large enough to generate overwash. Cross-barrier water-level slopes determine the rate and direction of transport, but these slopes are not necessarily linked to measures of storm intensity such as wave height or storm surge. If the slopes and

transport are landward, sand is safely sequestered in overwash deposits and (at least temporarily) appears in the stratigraphic record. But if slopes and transport are seaward, deposits on the ocean side are subject to immediate reworking after the storm. This mobile sand can aid in the immediate recovery of the beach by contributing sand to bars that weld onto the shoreface and spits that help close new breaches. Alternatively, it may be subject to alongshore transport and removal from the local barrier island sand budget. In extreme cases, sand may be transported seaward far beyond the depth of closure and effectively removed from the system.

6. Conclusions

We recorded time series of precise (±3.7 cm vertical) measurements of waves and water levels on both sides of an historically active overwash channel on the undeveloped northern Chandeleur Islands during inundation by Hurricane Isaac (28–30 August 2012). Subaerial island morphology was recorded by airborne lidar surveys conducted 7 months before and a few days after the storm. We simulated the morphology changes using the numerical model XBeach, forced with our water-level measurements (corrected for wave runup and wave-induced setup) and wave fields generated by a regional wave model. The measurements showed that soon after water levels were high enough to inundate the channel, water levels sloped offshore for most of the storm. Subaerial lidar data and field observations showed that three channels were eroded by 0.3 to 0.5 m, with no evidence of sediment accumulation on the landward side of the island. XBeach simulations forced with modeled waves and observed water levels generated net seaward transport and created erosional channels that dissected the island, depositing sand in the nearshore region on the ocean side. The model indicated that very little sand was deposited as overwash on the bay side, consistent with the measured poststorm topography. Numerical experiments found that sediment transport directions and magnitudes were sensitive to water levels and, in particular, water-level slopes. Specifically, higher ocean water levels resulted in traditional landward transport and development of overwash fans, and equal water levels cross-island resulted in a more uniform geomorphic response with no channelization, in contrast to the observed case of seaward transport resulting from higher bayside water levels. These results highlight the important influence of cross-barrier water levels on net transport during inundation events.

The northern Chandeleur Islands are unique in many respects, but the observations and model results described here have broader implications for other sites, as follows:

1. The methods we used to measure water levels in a region with no infrastructure during an extreme event were successful and could be applied elsewhere to extend our database of physical-forcing measurements during important geomorphic events.
2. The success of the XBeach model with minimal tuning indicated its utility for modeling morphologic response to events in beach and barrier environments elsewhere, contingent on correct boundary conditions.
3. Observed and modeled storm surge ebb was capable of driving significant seaward cross-barrier transport and producing scour channels, leaving deposits in the shallow nearshore on the ocean side.
4. The model results also showed that the maximum net landward transport did not always occur at the highest impact regime and that the morphologic changes associated with seaward sloping water levels were channel formation and deposition in the nearshore. Deposits associated with seaward transport may be more difficult to observe and are likely to be reworked in the active littoral zone, reducing the likelihood of their preservation. Hence, significant events may go unrecorded in the stratigraphic record, adding uncertainty in the reconstruction of storm recurrence intervals from sequences of overwash deposits.
5. Sensitivity runs suggest that landward water-level slopes produce a smoother final topography with either berm-top deposits or overwash deposits.

Acknowledgments

These data appear online in open-file reports and are available on request from the U.S. Geological Survey. Bathymetry measurements collected and processed by the USGS St. Petersburg Seafloor Mapping group were instrumental in completing this work, which was supported by the U.S. Geological Survey Coastal and Marine Geology Program. We thank N. DeWitt, K. Kelso, and B.J. Reynolds for outstanding help in the field, K. Guy for cartography, E.R. Thieler, A. Densmore, A. Ashton, and three anonymous reviewers for constructive comments on earlier drafts, and the U.S. Fish and Wildlife Service for permission to work in the Breton Island National Wildlife Refuge. Use of trade, product, or firm names is for descriptive purposes only and does not imply endorsement by the U.S. government.

References

Ashton, A. D., and A. C. Ortiz (2011), Overwash controls coastal barrier response to sea-level rise, in *Coastal Sediments '11, Proceedings of the Seventh International Symposium on Coast Engineering and Science of Coastal Sediment Processes, May 2–6, 2011*, 13 pp., ASCE, Miami, Fla.

Bendat, J. S., and A. G. Piersol (1986), *Random Data*, 2nd ed., 566 pp., John Wiley, New York.

Berg, R. (2012), Tropical Cyclone Report, Hurricane Isaac (AL092012), National Hurricane Center, National Oceanic and Atmospheric Administration. [Available at http://www.nhc.noaa.gov/data/tcr/AL092012_Isaac.pdf; 17 Feb.]

Birkemeier, W. A., E. W. Bichner, B. L. Scarborough, M. A. McConathy, and W. C. Eiser (1991), Nearshore profile response caused by Hurricane Hugo, *J. Coastal Res.*, *8*, 113–127.

Boothroyd, J. C., N. E. Friedrich, and S. R. McGinn (1985), Geology of microtidal coastal lagoons: Rhode Island, *Mar. Geol.*, *63*, 35–76.

Buynevich, I. V., and J. P. Donnelly (2006), Geological signatures of barrier breaching and overwash, Southern Massachusetts, USA, *J. Coastal Res.*, *39*, 112–116.
Cañizares, R., and J. L. Irish (2008), Simulation of storm-induced barrier island morphodynamics and flooding, *Coastal Eng.*, *55*(12), 1089–1101.
Carruthers, E. A., D. P. Lane, R. L. Evans, J. P. Donnelly, and A. D. Ashton (2013), Quantifying overwash flux in barrier systems: An example from Martha's Vineyard, Massachusetts, USA, *Mar. Geol.*, *343*(0), 15–28.
Cheung, K. F., L. Tang, J. P. Donnelly, E. M. Scileppi, K.-B. Liu, X.-Z. Mao, S. H. Houston, and R. J. Murnane (2007), Numerical modeling and field evidence of coastal overwash in southern New England from Hurricane Bob and implications for paleotempestology, *J. Geophys. Res.*, *112*, F03024, doi:10.1029/2006JF000612.
Chewen, B. M., S. D. Hoeksema, and I. C. Potter (2009), The divergent environmental characteristics of permanently-open, seasonally open and normally-closed estuaries of south-western Australia, *Estuarine Coastal Shelf Sci.*, *85*, 12–21.
Cooper, J. A. G. (2001), Geomorphological variability among microtidal estuaries from the wave-dominated South African coast, *Geomorphology*, *40*(1–2), 99–122.
Cowell, P. J., P. S. Roy, and R. A. Jones (1995), Simulation of large-scale coasts change using a morphological-behaviour model, *Mar. Geol.*, *126*, 45–61.
Dokka, R. K., G. F. Sella, and T. H. Dixon (2006), Tectonic control of subsidence and southward displacement of southeast Louisiana with respect to stable North America, *Geophys. Res. Lett.*, *33*, L23308, doi:10.1029/2006GL027250.
Donnelly, C., N. Kraus, and M. Larson (2006a), State of knowledge on measurement and modeling of coastal overwash, *J. Coastal Res.*, *22*(1), 965–991, doi:10.2112/04-0431.1.
Donnelly, C., R. Ranasinghe, and M. Larson (2006b), Numerical modeling of beach profile change caused by overwash, *Coastal Dyn.*, *2005*, 1–14, doi:10.1061/40855(214)56.
Donnelly, C., M. Larson, and H. Hanson (2009), A numerical model of coastal overwash, *Proc. ICE – Marit. Eng.*, *162*(3), 105–114.
Donnelly, J. P., et al. (2001a), 700 yr sedimentary record of intense hurricane landfalls in southern New England, *Geol. Soc. Am. Bull.*, *113*(6), 714–727.
Donnelly, J. P., S. Roll, M. Wengren, J. Butler, R. Lederer, and T. Webb III (2001b), Sedimentary evidence of intense hurricane strikes from New Jersey, *Geology*, *29*(7), 615–618.
Donnelly, J. P., J. Butler, S. Roll, M. Wengren, and T. Webb III (2004a), A backbarrier overwash record of intense storms from Brigantine, New Jersey, *Mar. Geol.*, *210*(1–4), 107–121.
Donnelly, J. P., P. Cleary, P. Newby, and R. Ettinger (2004b), Coupling instrumental and geological records of sea-level change: Evidence from southern New England of an increase in the rate of sea-level rise in the late 19th century, *Geophys. Res. Lett.*, *31*, L05203, doi:10.1029/2003GL018933.
Emery, K. O. (1969), *A Coastal Pond; Studied by Oceanographic Methods*, 80 pp., Elsevier, New York.
Emery, K. O., and J. F. Foster (1948), Water tables in marine beaches, *J. Mar. Res.*, *7*(3), 644–653.
Fearnley, S. M., M. D. Miner, M. Kulp, C. Bohling, and S. Penland (2009), Hurricane impact and recovery shoreline change analysis of the Chandeleur Islands, Louisiana, USA: 1855 to 2005, *Geo Mar. Lett.*, *29*, 455–466.
Figlus, J., N. Kobayashi, C. Gralher, and V. Iranzo (2011), Wave overtopping and overwash of dunes, *J. Waterw. Port Coastal Ocean Eng. Am. Soc. Civ. Eng.*, *137*, 26–33.
Galappatti, G., and C. B. Vreugdenhil (1985), A depth-integrated model for suspended sediment transport, *J. Hydraul. Res.*, *23*(4), 359–377.
Gayes, P. T. (1991), Post-Hurricane Hugo nearshore side scan sonar survey; Myrtle Beach to Folly Beach, South Carolina, *J. Coastal Res.*, *8*, 95–111.
Glahn, B., A. Taylor, N. Kurkowski, and W. A. Shaffer (2009), The role of the SLOSH model in National Weather Service storm forecasting, *Nat. Weather Dig.*, *33*(4), 3–14.
Goff, J. A., M. A. Allison, and S. P. S. Gulick (2010), Offshore transport of sediment during cyclonic storms), Hurricane Ike (2008) Texas Gulf Coast, USA, *Geology*, *38*, 351–354, doi:10.1130/G30632.1.
Guy, K. K., H. F. Stockdon, N. G. Plant, K. S. Doran, and K. L. M. Morgan (2013), Hurricane Isaac—Observations and Analysis of Coastal Change. *U.S. Geol. Surv. Open File Rep.,2013–1270*, 21 pp., U. S. Geological Survey, Reston, Va., doi:10.3133/ofr20131270.
Hart, D. E. (2009), Morphodynamics of non-estuarine rivermouth lagoons on high-energy coasts, *J. Coastal Res*, *SI56*, 1355–1359.
Hasselmann, K., et al. (1973), Measurements of wind-wave growth and swell decay during the Joint North Sea Wave Project (JONSWAP), *Ergnzungsheft zur Deutschen Hydrographischen Zeitschrift Reihe A*, *8*, 95.
Hayes, M. O. (1967), Hurricanes as geological agents, South Texas coast, *Am. Assoc. Pet. Geol. Bull.*, *51*(6), 937–942.
Hayes, M. O. (1975), Morphology of sand accumulations in estuaries, in *Estuarine Research*, edited by L. E. Cronin, pp. 3–22, Academic Press, New York.
Hayes, M. O. (1979), Barrier island morphology as a function of tidal and wave regime, in *Barrier Islands*: *From the Gulf of St. Lawrence to the Gulf of Mexico*, edited by S. P. Leatherman, pp. 1–28, Academic Press, New York.
Horn, D. P. (2002), Beach groundwater dynamics, *Geomorphology*, *48*, 121–146.
Inman, D. L., and C. E. Nordstrom (1971), On the tectonic and morphologic classification of coasts, *J. Geol.*, *79*(1), 1–21.
Jelesnianski, C. P., J. Chen, and W. A. Shaffer (1992), SLOSH: Sea, Lake, and Overland Surges from Hurricanes, *NOAA Tech. Rep. NWS 48*, Meteorological Development Laboratory, National Weather Service, National Oceanic and Atmospheric Administration, U. S. Department of Commerce, Silver Spring, Md., 71 p.
Jiménez, J. A., and A. Sánchez-Arcilla (2004), A long-term (decadal scale) evolution model for microtidal barrier systems, *Coastal Eng.*, *51*, 749–764, doi:10.1016/j.coastaleng.2004.07.007.
Kahn, J. H. (1986), Geomorphic recovery of the Chandeleur Islands, Louisiana, after a major hurricane, *J. Coastal Res.*, *2*, 337–344.
Kang, H.-Y., P. Nielsen, and D. J. Hanslow (1994), Watertable overheight due to wave runup on a sandy beach, Coastal Eng. 1994, in *Proceedings of the 24th International Conference on Coastal Eng.*, pp. 2115–2124, ASCE, Kobe, Japan.
Keim, B. D., R. A. Muller, and G. W. Stone (2007), Spatiotemporal patterns and return periods of tropical storm and hurricane strikes from Texas to Maine, *J. Clim.*, *20*, 3498–3507.
Kraus, N., A. Militello, and G. Todoroff (2002), Barrier breaching processes and barrier spit breach, Stone Lagoon, California, *Shore and Beach*, *70*(4), 21–28.
Laudier, N. A., E. B. Thornton, and J. MacMahan (2011), Measured and modeled wave overtopping on a natural beach, *Coastal Eng.*, *58*(9), 815–825.
Lavoie, D. (Ed.) (2009), Sand resources, regional geology, and coastal processes of the Chandeleur Islands coastal system—An evaluation of the Breton National Wildlife Refuge, U.S. Geological Survey Scientific Investigations Report 2009–5252, 180 p.
Lavoie, D., J. G. Flocks, J. L. Kindinger, A. H. Sallenger Jr., and D. C. Twichell (2010), Effects of building a sand barrier berm to mitigate the effects of the Deepwater Horizon oil spill on Louisiana marshes, *U.S. Geol. Surv. Open File Rep., 2010–1108*, 7 p.
Leatherman, S. P. (1979), Migration of Assateague Island, Maryland, by inlet and overwash processes, *Geology*, *7*(2), 104–107.

Leatherman, S. P. (1981), *Overwash Processes*, vol. 58, 376 pp., Benchmark Papers in Geology, Hutchinson Ross.
Leatherman, S. P. (1983), Barrier dynamics and landward migration with Holocene sea-level rise, *Nature*, *301*, 415–417.
Lennon, G. (1991), The nature and causes of hurricane-induced ebb scour channels on a developed shoreline, *J. Coastal Res.*, *237–248*, doi:10.2307/25735418.
Li, L., D. A. Barry, J. Y. Parlange, and C. B. Pattiaratchi (1997), Beach water table fluctuations due to wave run-up: Capillarity effects, *Water Resour. Res.*, *33*, 935–945, doi:10.1029/96WR03946.
Lindemer, C. A., N. G. Plant, J. A. Puleo, D. M. Thompson, and T. V. Wamsley (2010), Numerical simulation of a low-lying barrier island's morphological response to Hurricane Katrina, *Coastal Eng.*, *57*, 985–995, doi:10.1016/j.coastaleng.2010.06.004.
Long, J. W., A. T. M. de Bakker, and N. G. Plant (2014), Scaling coastal dune elevation changes across storm-impact regimes, *Geophys. Res. Lett.*, *41*, 2899–2906, doi:10.1002/2014GL059616.
Lorenzo-Trueba, J., and A. D. Ashton (2014), Rollover, drowning, and discontinuous retreat: Distinct modes of barrier response to sea-level rise arising from a simple morphodynamic model, *J. Geophys. Res. Earth Surf.*, *119*, 779–801, doi:10.1002/2013JF002941.
Louisiana Department of Natural Resources (2010), U.S. Army Corps of Engineers joint permit application for work within the Louisiana coastal zone. [Available at http://www.lacpra.org/assets/docs/Berm%20File/Berm%20Permit%20Application.pdf.]
McBride, R. A., S. Penland, M. W. Hiland, S. J. Williams, K. A. Westphal, B. E. Jaffe, and A. H. Sallenger Jr. (1992), Chapter 4: Analysis of Barrier Island Shoreline Change in Louisiana from 1853 to 1989, in *Atlas of Shoreline Changes in Louisiana from 1853 to 1989*, *U.S. Geol. Surv.*, Miscellaneous Investigations Series I-2150-A, edited by S. J. Williams, S. Penland, and A. H. Sallenger Jr., pp. 36–97, Geological Survey and Louisiana State Univ., Reston, Va.
McBride, R. A., M. R. Byrnes, and M. W. Hiland (1995), Geomorphic response-type model for barrier coastlines: A regional perspective, *Mar. Geol.*, *126*(1–4), 143–159, doi:10.1016/0025-3227(95)00070-F.
McBride, R. A., et al. (2013), Morphodynamics of barrier systems: A synthesis, in *Treatise on Geomorphology*, edited by J. Shroder and D. J. Sherman, pp. 166–244, Academic Press, San Diego.
McCall, R. T., J. S. M. Van Thiel de Vries, N. G. Plant, A. R. Van Dongeren, J. A. Roelvink, D. M. Thompson, and A. J. H. M. Reniers (2010), Two-dimensional time dependent hurricane overwash and erosion modeling at Santa Rosa Island, *Coastal Eng.*, *57*, 668–683, doi:10.1016/j.coastaleng.2010.02.006.
Morton, R. A., and A. H. Sallenger Jr. (2003), Morphological impacts of extreme storms on sandy beaches and barriers, *J. Coastal Res.*, *19*(3), 560–573.
Morton, R., N. A. Buster, and M. D. Krohn (2002), Surface controls on historical subsidence rates and associated wetland loss in south-central Louisiana, *Trans. Gulf Coastal Assoc. Geol.*, *52*, 767–778.
Nielsen, P. (1990), Tidal dynamics of the water table in beaches, *Water Resour. Res.*, *26*, 2127–2134.
Nielsen, P. (1999), Groundwater dynamics and salinity in coastal barriers, *J. Coastal Res.*, *15*(3), 732–740.
Olabarrieta, M., J. C. Warner, and N. Kumar (2011), Wave-current interaction in Willapa Bay, *J. Geophys. Res.*, *116*, C12014, doi:10.1029/2011JC007387.
Otvos, E. G. (1986), Island evolution and "stepwise retreat": Late Holocene transgressive barriers, Mississippi delta coast—Limitations of a model, *Mar. Geol.*, *72*, 325–340, doi:10.1016/0025-3227(86)90126-X.
Otvos, E. G., and G. A. Carter (2013), Regressive and transgressive barrier islands on the North-Central Gulf Coast—Contrasts in evolution, sediment delivery, and island vulnerability, *Geomorphology*, *198*, 1–19.
Park, Y. H., and B. L. Edge (2010), An empirical model to estimate overwash, *J. Coastal Res.*, *26*(6), 1157–1167.
Peng, M., L. Xie, and L. J. Pietrafesa (2004), A numerical study of storm surge and inundation in the Croatan-Albemarle-Pamlico Estuary System, *Estuarine Coastal Shelf Sci.*, *59*(1), 121–137.
Penland, S., and K. E. Ramsey (1990), Relative sea-level rise in Louisiana and the Gulf of Mexico 1908–1988, *J. Coastal Res.*, *6*, 323–342.
Penland, S., J. R. Suter, and R. Boyd (1985), Barrier island arcs along abandoned Mississippi River deltas, *Mar. Geol.*, *63*, 197–233, doi:10.1016/0025-3227(85)90084-2.
Pierce, J. W. (1970), Tidal inlets and washover fans, *J. Geol.*, *78*, 230–234.
Pilkey, O. H. (2003), *Celebration of the World's Barrier Islands*, 400 pp., Columbia Univ. Press, New York.
Plant, N. G., and K. K. Guy (2013a), Change in the length of the northern section of the Chandeleur Islands oil berm, September 5, 2010, through September 3, 2012, *U.S. Geol. Surv. Open File Rep., 2013–1074*, 9 p.
Plant, N. G., and K. K. Guy (2013b), Change in the length of the middle section of the Chandeleur Islands oil berm, November 17, 2010, through September 6, 2011, *U.S. Geol. Surv. Open File Rep., 2013–1075*, 8 p.
Plant, N. G., K. T. Holland, and J. A. Puleo (2002), Analysis of the scale of errors in nearshore bathymetric data, *Mar. Geol.*, *191*(1), 71–86.
Plant, N. G., J. Flocks, H. F. Stockdon, J. W. Long, K. Guy, D. M. Thompson, J. M. Cormier, C. G. Smith, J. L. Miselis, and P. S. Dalyander (2014), Predictions of barrier island berm evolution in a time-varying storm climatology, *J. Geophys. Res. Earth Surf.*, *119*, 300–316, doi:10.1002/2013JF002871.
Poppe, L., S. Williams, and V. Paskevich (2005), U.S. Geological Survey east-coast sediment analysis; procedures, database, and GIS data, *U.S. Geol. Surv. Open File Rep., 2005–1001*, DVD-ROM, supersedes OFR 00–358. [Also available at http://pubs.usgs.gov/of/2005/1001/index.htm.]
Ranasinghe, R., C. Pattiaratchi, and G. Masselink (1999), A morphodynamic model to simulate the seasonal closure of tidal inlets, *Coastal Eng.*, *37*(1), 1–36.
Raubenheimer, B., S. Elgar, and R. T. Guza (1998), Estimating wave heights from pressure measured in sand bed, *J. Waterw. Port Coastal, Ocean Eng.*, *124*, 151–154.
Rego, J. L., and C. Li (2010), Storm surge propagation in Galveston Bay during Hurricane Ike, *J. Mar. Syst.*, *82*, 265–279.
Ris, R. C., N. Booij, and L. H. Holthuijsen (1999), A third-generation wave model for coastal regions), 2. Verification, *J. Geophys. Res.*, *104*, 7667–7681, doi:10.1029/1998JC900123.
Roelvink, D., A. Reniers, A. van Dongeren, J. van Thiel de Vries, R. McCall, and J. Lescinski (2009), Modelling storm impacts on beaches, dunes and barrier islands, *Coastal Eng.*, *56*, 1133–1152, doi:10.1016/j.coastaleng.2009.08.006.
Rosati, J. D., and G. W. Stone (2009), Geomorphologic evolution of barrier islands along the northern U.S. Gulf of Mexico and implications for engineering design in barrier restoration, *J. Coastal Res.*, *25*(1), 8–22.
Roy, P. S., R. J. Williams, A. R. Jones, I. Yassini, P. J. Gibbs, B. Coates, R. J. West, P. R. Scanes, J. P. Hudson, and S. Nichol (2001), Structure and function of south-east Australian estuaries, *Estuarine Coastal Shelf Sci.*, *53*(3), 351–384.
Sallenger, A. H., Jr. (2000), Storm impact scale for barrier islands, *J. Coastal Res.*, *16*, 890–895, doi:10.2307/4300099.
Sheng, Y. P., Y. Zhang, and V. A. Paramygin (2010), Simulation of storm surge, wave, and coastal inundation in the Northeastern Gulf of Mexico region during Hurricane Ivan in 2004, *Ocean Modell.*, *35*, 314–331, doi:10.1016/j.ocemod.2010.09.004.
Soulsby, R. (1997), *Dynamics of Marine Sands: A Manual for Practical Applications*, Thomas Telford, London.
Splinter, K. D., and M. L. Palmsten (2012), Modeling dune response to an East Coast Low, *Mar. Geol.*, *329–331*, 46–57, doi:10.1016/j.margeo.2012.09.005.

Stockdon, H. F., A. H. Sallenger Jr., R. A. Holman, and P. A. Howd (2007), A simple model for the spatially-variable coastal response to hurricanes, *Mar. Geol.*, *238*, 1–20, doi:10.1016/j.margeo.2006.11.004.

Stockdon, H. F., K. J. Doran, D. M. Thompson, K. L. Sopkin, N. G. Plant, and A. H. Sallenger (2012), National assessment of hurricane-induced coastal erosion hazards—Gulf of Mexico, *U.S. Geol. Surv. Open File Rep., 2012–1084*, 51 p.

Stolper, D., J. H. List, and E. R. Thieler (2005), Simulating the evolution of coastal geomorphology and stratigraphy with a new morphological-behavior model (GEOMBEST), *Mar. Geol.*, *218*, 17–36.

Stoker, J. J. (1957), Water Waves, Interscience, New York.

Taylor, J. R. (1997), *An Introduction to Error Analysis*, 2nd ed., 327 pp., University Science Books, Calif.

Tedesco, L. P., H. R. Wanless, L. A. Scusa, J. A. Risi, and S. Gelsanliter (1995), Impact of Hurricane Andrew on South Florida's Sandy Coastlines, *J. Coastal Res.*, *21*, 59–82, doi:10.2307/25736001.

Thieler, E. R., and D. M. Bush (1991), Hurricanes Gilbert and Hugo send powerful messages for coastal development, *J. Geol. Educ.*, *39*, 291–298.

Thieler, E. R., D. M. Bush, and O. H. Pilkey (1989), Shoreline response to Hurricane Gilbert: Lessons for coastal management, in *Proceedings of the Sixth Symposium on Coastal and Ocean Management*, pp. 765–775, ASCE, New York.

Thornton, E. B., and R. T. Guza (1983), Transformation of wave height distribution, *J. Geophys. Res.*, *88*, 5925–5938, doi:10.1029/JC088iC10p05925.

Tolman, H. (2008), A mosaic approach to wind wave modeling, *Ocean Modell.*, *25*(1), 35–47.

Twichell, D. C., J. G. Flocks, E. A. Pendleton, and W. E. Baldwin (2013), Geologic controls on regional and local erosion rates of three northern Gulf of Mexico barrier-island systems, *J. Coastal Res.*, *63*, 32–45.

Twichell, D. E., W. B. Pendleton, and J. Flocks (2009), Subsurface control on seafloor erosion processes offshore of the Chandeleur Islands Louisiana, *Geo Mar. Lett.*, *29*, 349–358.

Waddell, E. (1976), Swash-groundwater-beach profile interactions, in *Beach and Nearshore Sedimentation*, edited by R. A. Davis Jr. and R. L. Ethington, pp. 115–125, Society of Economic Paleontologists and Minerologists, Tulsa, Okla.

Zecchetto, S., G. Umgiesser, and M. Brocchini (1997), Hindcast of a storm surge induced by local real wind fields in the Venice Lagoon, *Cont. Shelf Res.*, *17*(12), 1513–1538.